Integrated optical Ti:Er:LiNbO₃ distributed Bragg reflector laser with a fixed photorefractive grating

Ch. Becker, A. Greiner, Th. Oesselke, A. Pape, W. Sohler, and H. Suche

Angewandte Physik, Universität-GH Paderborn, Warburger Strasse 100, D-33098 Paderborn, Germany

For the first time to the authors' knowledge, an integrated optical distributed Bragg reflector laser with a fixed photorefractive grating in LiNbO₃ is demonstrated. Sample preparation, grating fabrication, and laser characteristics are reported. The device is pumped by a fiber pigtailed laser diode ($\lambda_p \approx 1480$ nm) through the Bragg grating in a double-pass configuration, yielding an emission in the backward direction at $\lambda = 1531.7$ nm. The laser threshold is 40 mW; as much as 5 mW of output power has been obtained at 110 mW of launched pump power in cw operation.   © 1998 Optical Society of America

    OCIS codes: 050.7330, 230.1480, 230.3120.

Recently, integrated optical Ti:Er:LiNbO₃ distributed Bragg reflector (DBR) lasers were developed with holographically defined ion-beam-etched surface gratings for narrow-band optical feedback.[1] However, DBR lasers with etched surface gratings suffer from several drawbacks: The fabrication technology is complicated.[2] Grating inhomogeneities induce extra losses of the lasing mode. The overlap of the grating and the lasing mode is small, requiring a long interaction length. The pump mode is partially coupled to substrate modes, which results in high extra losses; therefore pumping through the Bragg grating is not possible.

Photorefractive gratings, as used successfully in fiber-optic DBR and distributed-feedback lasers,[3] are a promising alternative to etched gratings, avoiding all the drawbacks mentioned above. We report in this Letter what we believe is the first DBR waveguide laser ($\lambda = 1531$ nm) in Er-diffusion-doped LiNbO₃ with a fixed photorefractive grating in an Fe-doped Ti-diffused strip waveguide; the device is pumped by a laser diode ($\lambda_p \approx 1480$ nm).

A schematic diagram of the laser is presented in Fig. 1. The laser was fabricated in a 70-mm-long X-cut LiNbO₃ substrate that had been Er-doped over 43 mm by indiffusion of a 15-nm-thick, vacuum-deposited Er layer at 1120 °C during 120 h. Subsequently, the remaining surface was Fe-diffusion doped (33 nm, 1060 °C, 72 h) to increase the photorefractive sensitivity for grating fabrication. Finally, an 8-μm wide, 97-nm-thick photolithographically defined Ti stripe parallel to the c axis was indiffused, forming the optical channel guide. The sample was annealed at 500 °C for 3 h in flowing Ar (0.5 L/min) to enhance the Fe²⁺/Fe³⁺ ratio, which determines the photorefractive susceptibility.

The laser resonator consisted of a broadband dielectric high reflector on the polished waveguide end face of the Er-doped section and of a narrow-band grating reflector in the Fe-doped section. The end face on the right-hand side was antireflection coated for fiber butt coupling. Finally, the upper and lower sample surfaces were antireflection coated as well to avoid interference effects during the grating fabrication.

The grating was written by use of a holographic setup with an Ar laser ($\lambda = 488$ nm). The periodic illumination led to a corresponding excitation of electrons from Fe²⁺ states; they were redistributed by drift, diffusion, and the photovoltaic effect in LiNbO₃. The last-named is the dominant transport mechanism along the optical c axis. Finally, the electrons were trapped by acceptor states (Fe³⁺ ions) in areas of low optical intensity. This redistribution generated a periodic space-charge field, which modulated the refractive index by means of the electro-optic effect and in this way generated a narrow-band Bragg-reflector grating.

A grating fabricated at room temperature is not stable. Therefore our grating was written by a 2-h exposure at 170 °C. At this temperature protons in the crystal become mobile and compensate for the periodic electronic space charge.[4,5] After cooling to room temperature, these ions were frozen at their high-temperature positions. Homogeneous illumination with the collimated beam of a 100-W halide lamp then led to a nearly homogeneous redistribution of the electronic charge, in this way developing a stable ionic grating as a replica of the inverse polarity of the initial electronic space-charge distribution.
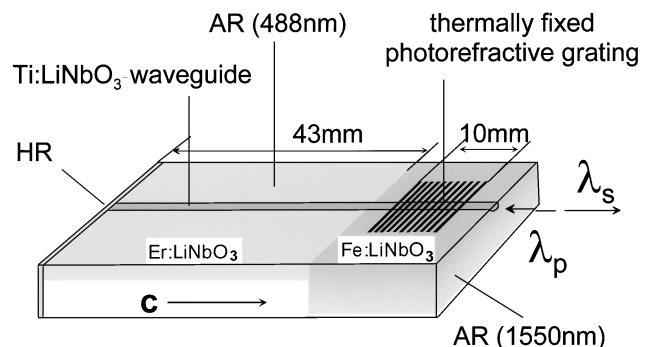

Fig. 1. Schematic structure of the Ti:Er:LiNbO₃ DBR waveguide laser with a photorefractive grating in the Fe-doped section. HR, highly reflecting dielectric mirror; AR, antireflection coating.

The laser was first characterized as a passive device. The Er and the Fe concentration profiles are Gaussian-like, with surface concentrations of 1.15×10^{20} (4.7×10^{19}) cm^{-3} and $1/e$ penetration depths of 4.7 (63) μm for Er (Fe), respectively.

The Ti-diffused optical waveguide was single mode for wavelengths near 1550 nm, with the fundamental TM mode slightly larger than the TE mode [8.5 μm (width) $\times$ 4.8 μm (depth) and 8.4 μm $\times$ 4.5 μm, respectively]. The scattering losses were as low as 0.02 dB/cm in a reference channel without Er doping. For the Er-doped waveguide, scattering losses of ~0.2 dB/cm were estimated by comparison of modeled and the measured laser results. Absorption coefficients for the Er-doped section were not measured but can be estimated to be ~1.4 (8.5) dB/cm at 1480- (1531-) nm wavelength for TE-polarized light. These values can be inferred from mode-size and absorption cross-section measurements for α-polarized light [both $E, B \perp c$, in contrast to σ-polarized light ($E \perp c$ only)].

The high reflector had reflectivities of ~80% for both signal and pump wavelengths. In this way double-pass pumping of improved absorption efficiency was achieved. The mirror consisted of only six layers so it could withstand the rapid thermal cycling during fixing of the grating. We determined the spectral characteristics of the holographically written grating by slightly pumping the device and measuring the backscattered amplified spontaneous emission from the Er-doped section transmitted through the grating. This measurement yielded a minimum transmission of ~40%, corresponding to a reflectivity of ~60%. Because of an electronic compensation of the ionic grating, the reflectivity dropped slowly as function of time. However, this compensation could easily be reversed by another homogeneous illumination. Figure 2 shows the specific result measured for the optimum output coupling of the DBR laser. The half-width of the grating was ~0.11 nm.

To operate the DBR laser we used a pigtailed diode laser ($\lambda_p \approx 1480$ nm) for pumping. A fiber-optic wavelength-division multiplexer launched as much as 110 mW of pump power into the DBR laser and simultaneously extracted the laser emission in the backward direction. Laser emission could be achieved in both TE and TM polarization. The actual polarization was determined by the location of the axial eigenmodes with respect to the peak reflectivity of the Bragg reflector. By thermal drift, alternating TE and TM emission could be observed.

TE polarization for both pump and emission yielded the maximum output power (Fig. 3), as the smaller TE modes resulted in better overlap with the Er concentration profile. To suppress TM emission we deposited a stripe of Ag paste operating as a TE-pass polarizer across the waveguide close to the high reflector. The grating bandwidth of ≈ 0.11 nm led to the simultaneous emission of three longitudinal modes (Fig. 3, inset) with a central wavelength of 1531.7 nm. The maximum TE-polarized output power of 5 mW was measured for a grating reflectivity of ~45%. The saturation of the output power at

high pump power levels was due to a change of the pump spectrum (broadening and shifting to longer wavelengths) caused by backreflections into the non-isolated diode laser. As a result the pump absorption efficiency and hence the slope efficiency of the DBR laser were reduced.

After the laser characterization as described above, a single-mode standard telecommunication fiber was glued to the antireflection-coated waveguide end face (pigtailing); finally, the sample was packaged in a temperature-stabilized aluminum box. After packaging of the sample, we monitored the output power of the DBR laser and the reflectivity of the Bragg grating as a function of time to determine the optimum output coupling. Starting with a reflectivity of ~60% (Fig. 4), we measured a maximum TE-polarized output power of 3.7 mW for a grating reflectivity of ~40%. In comparison with the results presented in Fig. 3, the maximum output power was reduced because of nonideal fiber pigtailing.

Modeling results predict a significant potential for improvements. Assuming 0.1-dB/cm waveguide scattering losses, achievement of optimized Er diffusion
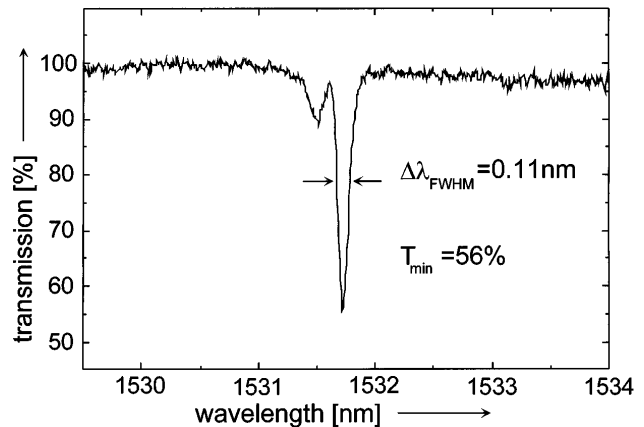

Fig. 2. Transmission of a fixed photorefractive grating versus wavelength.
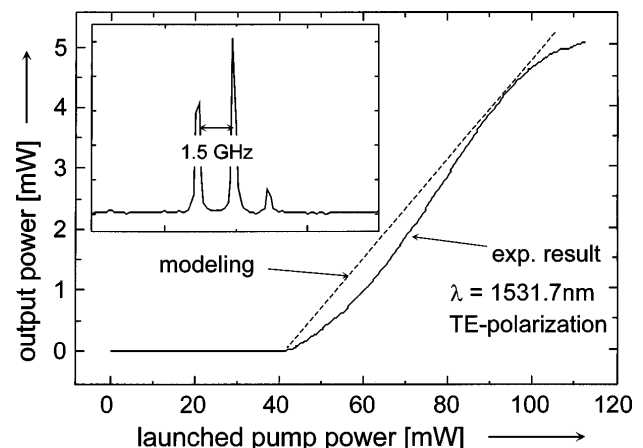

Fig. 3. Power characteristics of the DBR laser. Inset, axial mode spectrum (TE polarized).
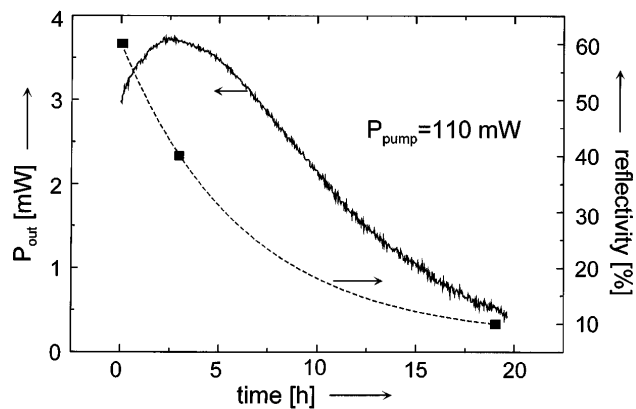
Fig. 4.   Output power of the pigtailed and packaged DBR laser and reflectivity of the Bragg grating as function of time (filled squares, measured response; dashed curve, fitted exponential decay).

plications the slow electronic compensation of the ionic space-charge grating will have to be suppressed to stabilize the Bragg response.   This problem will be investigated.

and output coupling through the grating up to 32% slope efficiency and 15 mW of output power at 80 mW of launched pump power seem to be feasible at the same emission wavelength.   However, for practical ap-

References

1. J. Söchtig, R. Gross, I. Baumann, W. Sohler, H. Schütz, and R. Widmer, Electron. Lett. **31,** 551 (1995).
2. J. Söchtig, H. Schütz, R. Widmer, H. W. Lehmann, and R. Gross, in *Nanofabrication Technologies and Device Integration,* W. Karthe, ed., Proc. SPIE **2213,** 97 (1994).
3. J. Hübner, P. Varming, and M. Kristensen, Electron. Lett. **33,** 139 (1997).
4. J. J. Amodei and D. L. Staebler, Appl. Phys. Lett. **18,** 540 (1971).
5. K. Buse, S. Breer, K. Peithmann, S. Kapphan, M. Gao, and E. Krätzig, Phys. Rev. B **56,** 1225 (1997).